

Grundmannite, CuBiSe_2 , the Se-analogue of emplectite, a new mineral from the El Dragón mine, Potosí, Bolivia

HANS-JÜRGEN FÖRSTER^{1,*}, LUCA BINDI² and CHRIS J. STANLEY³

¹ Helmholtz Centre Potsdam German Research Centre for Geosciences GFZ, D-14473 Potsdam, Germany

*Corresponding author, e-mail: hans-jürgen.förster@gfz-potsdam.de

² Dipartimento di Scienze della Terra, Università degli Studi di Firenze, Via G. La Pira 4, I-50121 Firenze, Italy

³ Department of Earth Sciences, Natural History Museum, Cromwell Road, London SW7 5BD, UK

Abstract: Grundmannite, ideally CuBiSe_2 , is a new mineral species from the El Dragón mine, Department of Potosí, Bolivia. It either fills small shrinkage cracks or interstices in brecciated krut'aite–penroseite solid solutions or forms independent grains in the matrix. Grain size of the anhedral to subhedral crystals is usually in the range 50–150 μm , but may approach 250 μm . Grundmannite is usually intergrown with watkinsonite and clausthalite; other minerals occasionally being in grain-boundary contact comprise quartz, dolomite, native gold, eldragónite, eskebornite, umangite, klockmannite, Co-rich penroseite, and three unnamed phases of the Cu–Hg–Pb–Bi–Se system, among which is an as-yet uncharacterized species with the ideal composition $\text{Cu}_4\text{Pb}_2\text{HgBi}_4\text{Se}_{11}$. Grundmannite is non-fluorescent, black and opaque with a metallic lustre and black streak. It is brittle, with an irregular fracture and no obvious parting. Some grains display a perfect {001} cleavage. The VHN_{20} values range from 45 to 61 (mean 53) kg mm^{-2} , which equates to a Mohs hardness of 2 to 2½. In plane-polarized incident light, grundmannite is weakly bireflectant and weakly pleochroic, from cream to light grey, and shows no internal reflections. Between crossed polarisers, grundmannite is distinctly anisotropic, with light-brown to brown rotation tints. The reflectance values in air for the COM standard wavelengths are: 41.0–43.4 (470 nm), 41.8–45.1 (546 nm), 42.1–45.7 (589 nm), and 42.5–46.2 (650 nm). Electron probe micro-analyses yielded a mean composition Cu 14.88, Pb 1.23, Hg 0.07, Ni 0.05, Bi 44.90, Se 38.92, total 100.05 wt.%. The mean empirical formula, normalized to 4 atoms per formula unit (apfu), is $\text{Cu}_{0.99}(\text{Bi}_{0.91}\text{Pb}_{0.02})_{\Sigma 0.93}\text{Se}_{2.08}$ ($n = 19$). The ideal formula is CuBiSe_2 , which requires (in wt.%) Cu 14.76, Bi 48.55, Se 36.69, sum 100.00. Grundmannite is orthorhombic, space group $Pnma$, with $a = 6.6362(5)$, $b = 4.2581(3)$, $c = 15.3691(9)$ Å, $V = 434.29(5)$ Å³, and $Z = 4$. Density, calculated on the basis of the mean chemical composition and unit-cell parameters derived from the single-crystal X-ray study, is 6.582 g cm^{-3} . The five strongest X-ray powder-diffraction lines [d in Å (I/I_0) (hkl)] are: 3.4901 (50) (111), 3.3180 (70) (200), 3.2746 (100) (013), 2.4923 (45) (015), and 2.3307 (50) (213). The crystal structure of grundmannite is topologically identical to that of emplectite, CuBiS_2 , with the two independent sulfur positions occupied by Se, thus being the Se-isotype of emplectite. In the structure, Bi forms BiSe_3 trigonal pyramids (with two additional longer distances) and Cu nearly regular CuSe_4 tetrahedra. Grundmannite is a primary mineral, deposited from an oxidizing low-temperature hydrothermal fluid at the waning stage of selenide-mineral formation at El Dragón, at a $f\text{Se}_2/f\text{S}_2$ ratio greater than unity and in the presence of hematite, conditions typically prevailing during the formation of telethermal vein-type selenide deposits. The mineral was named after Günter Grundmann, in recognition of his pioneering work on the El Dragón mine.

Key-words: grundmannite; new mineral species; chemical composition, crystal structure; bismuth; copper; selenium; Cu–Hg–Pb–Bi–Se system; $\text{Cu}_4\text{Pb}_2\text{HgBi}_4\text{Se}_{11}$; El Dragón; Bolivia.

1. Introduction

In the Andes of South America, the province of La Rioja in Argentina hosts one of the most important selenium mineralizations on Earth (e.g., Paar *et al.*, 2012). Bolivia is well known for two minor, but scientifically interesting selenide occurrences: Pacajake, district of Hiaco de Charcas, and El Dragón, Province of Quijarro, both in the Department of Potosí. The geology and ore mineralization of the El Dragón mine was first explored in detail by Grundmann *et al.* (1990); it subsequently received further attention as

the type locality of eldragónite, $\text{Cu}_6\text{BiSe}_4(\text{Se}_2)$, and for two unnamed species of the Cu–Hg–Pb–Bi–Se system (Paar *et al.*, 2012), and the new secondary Pb–Bi–Cu selenite favreauite, $\text{PbBiCu}_6\text{O}_4(\text{SeO}_3)_4(\text{OH}) \cdot \text{H}_2\text{O}$ (Mills *et al.*, 2014).

A renewed comprehensive study of a large number of ore-bearing samples from El Dragón, collected during two field campaigns in 1987 and 1988 by a research team from the Technische Universität München, Germany, revealed the presence of another Cu–Bi sulfosalt with the composition CuBiSe_2 , constituting the Se-analogue of emplectite,

CuBiSe₂. The description of this new selenium mineral, grundmannite, forms the subject of this paper. The natural existence of a mineral of the composition CuBiSe₂ was first implied from quantitative microprobe data of unknown species present in the complex Se mineralization at Altenberg a.d. Rax (Steiermark, Austria), but neither compositional nor structural data were provided (Niedermayr *et al.*, 1997). Interestingly, the existence of a cubic phase with composition CuBiSe₂ was already mentioned by Zhuze *et al.* (1958). Förster *et al.* (2005) described the occurrence of a bohdanowiczite-like compound from Niederschlema–Alberoda (Erzgebirge, Germany) having variable (Ag/Cu) contents, with chemical compositions ranging from bohdanowiczite *s.s.* (AgBiSe₂) to phases having an intermediate composition between the bohdanowiczite end-member composition and ideal CuBiSe₂. The empirical formula for the most Cu-rich phase is (Cu_{0.52}Ag_{0.47})_{Σ0.99}Bi_{1.01}Se_{1.99}, based on 4 *apfu*.

The new species grundmannite and its name have been approved by the Commission on New Minerals, Nomenclature and Classification (CNMNC) of the IMA, proposal 2015–038. The holotype specimen, which is the section from which the grain used for crystal-structure determination was obtained, is deposited in the collections of the Natural History Museum, London, catalogue number BM 2015, 33. Cotype material, consisting of a grundmannite-bearing section, is housed within the Mineralogische Staatssammlung München, Museum “Reich der Kristalle” (Munich), under the inventory number MSM 73584. The mineral name is in honour of Günter Grundmann (b. 1947), in recognition of his pioneering work on the El Dragón mine (*e.g.*, Grundmann *et al.*, 1990).

2. Geological setting

The El Dragón selenide occurrence is situated in southwestern Bolivia, in the Cordillera Oriental, some 30 km southwest of Cerro Rico de Potosí. The abandoned El Dragón mine (entrance and dump) is located 19° 49' 23.90" S (latitude), 65° 55' 00.60" W (longitude), at an altitude of 4,160 m above sea level. It is about 4 km east of the Porco Caldera hosting one of the largest Ag–Zn–Pb–Sn deposits in Bolivia (Cunningham *et al.*, 1993). The Porco mining district has a long history of production, beginning in pre-Columbian times when Indians mined it for silver. The very small longitudinal extension (maximum 15 m-long gallery) of the El Dragón Se ore vein and its low Ag content (0.06 wt.% Ag) have probably discouraged further exploitation of the occurrence.

The adit of the El Dragón mine is on the orographic left side of the Rio Jaya Mayu, cutting through a series of thinly stratified, pyrite-rich black shales and reddish-grey, hematite-bearing siltstones of probably Devonian age, dipping 40° to the north. The almost vertical ore vein is located in the centre of a 1.5 m-wide shear zone (average trend 135 degrees) with shifts of a few cm. In 1988, the Se mineralization consisted of a single vein, ranging mostly from 0.5 to 2 cm in thickness, with sporadic bulges of up to 6 cm.

3. Occurrence and physical properties

The El Dragón mineralization is composed of a complex assemblage of partially rare primary and secondary minerals, among which Se-bearing phases are most prominent. The full list of minerals recorded from El Dragón is given at <http://www.mindat.org/loc-353.html>. Grundmann *et al.* (1990) and Paar *et al.* (2012) provided detailed descriptions of the entire mineralization. Here we focus on grundmannite and associated primary minerals of the system Cu–Hg–Pb–Bi–Se. A comprehensive discussion of the origin of the El Dragón mineralization will form the subject of a forthcoming paper.

During this study, a total of 125 polished thick sections of average size 2 × 2 cm and average weight 8 g and several polished vein sections of up to 4 cm in thickness with adhesive wall-rock fragments were examined macroscopically and microscopically. Grundmannite was detected in only 10 % of the inspected thick sections. Other associated Cu–Bi-bearing selenides are comparatively more frequent. Thus, watkinsonite (Cu₂PbBi₄Se₈) was present in almost all inspected samples, and eldragónite in about two thirds of the sections.

The appearance and mineral associations of grundmannite and other Bi-selenides are shown in Figs 1 and 2, reporting a collection of optical micrographs and back-scattered electron (BSE) images, respectively.

Grundmannite commonly forms sub- to anhedral grains up to 150 μm in size, typically intergrown with claustralite (PbSe; Figs. 1a–c and 2a–b) and associated with krut'aite–penroseite solid solutions (Cu₂Se–Ni₂Se; Fig. 1a–d). These solid solutions usually form systematically zoned grains, with Cu-rich compositions resembling krut'aite in the cores evolving towards more Ni–(Co)-rich compositions in the direction of the grain margins, with penroseite *s.s.* at the outermost rims. Grundmannite also appears as aggregates of irregularly shaped grains of several hundreds of μm across associated with the same species as above (Fig. 1b). Grundmannite occasionally shows parallel intergrowths of grains, implied from serrated prismatic grain surfaces. Intergrowths with watkinsonite are common (Fig. 1a–d). Other minerals occasionally being in contact with grundmannite comprise quartz, dolomite, native gold (Fig. 1c), eldragónite, eskebornite (CuFeSe₂), umangite (Cu₃Se₂), klockmannite (CuSe), discrete grains of Co-rich penroseite, unnamed phases “A” and “B” of Paar *et al.* (2012), and a newly discovered species of the Cu–Hg–Pb–Bi–Se system termed phase “C” (*cf.* section Chemical composition). Petrovicite rarely precipitated in the surroundings of CuBiSe₂. Grundmannite partially replaces umangite, klockmannite, eskebornite and, possibly, native gold and is itself altered by late fracture-filling chalcopyrite (Fig. 1d). Secondary minerals in the neighbourhood of grundmannite encompass chalcomenite, favreauite, molybdomenite, ahlfeldite, olsacherite, schmiederite, goethite, lepidocrocite, alunite, and late klockmannite.

About half of the identified grundmannite grains cement (usually together with claustralite, watkinsonite

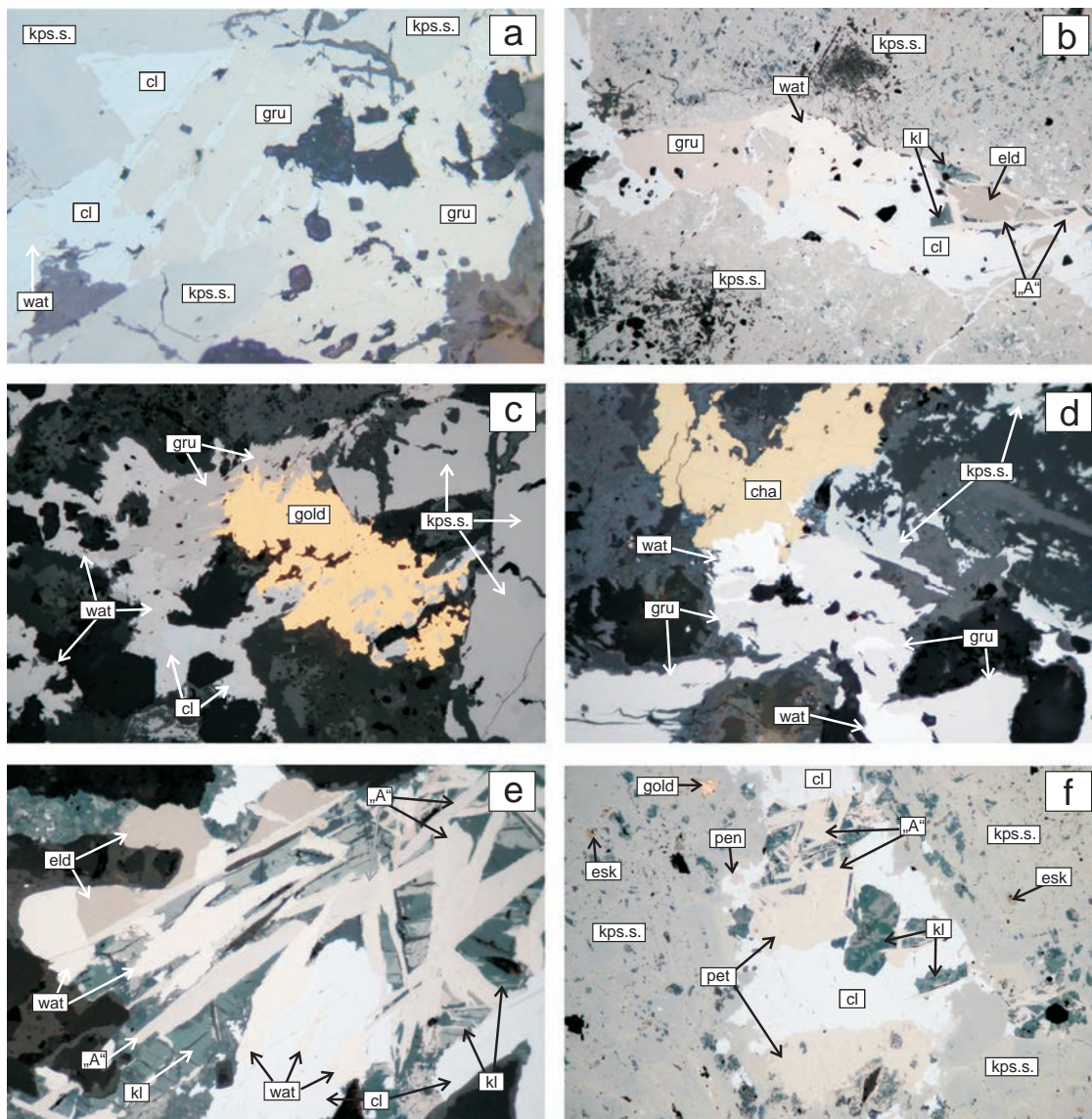


Fig. 1. Reflected-light photomicrographs of (a) the grain of grundmannite, from which the structural and reflectance data were obtained (horizontal field (h.f.) $\sim 250 \mu\text{m}$); (b) grundmannite, watkinsonite, eldragonite, klockmannite, and clausthalite as fracture filling in intensely zoned krut'aite–penroseite solid solution (h.f. $\sim 500 \mu\text{m}$); (c) grundmannite + clausthalite + watkinsonite replacing native Au (h.f. $\sim 500 \mu\text{m}$); (d) grundmannite + watkinsonite + krut'aite–penroseite replaced by chalcopyrite along fractures (h.f. $\sim 200 \mu\text{m}$); (e) intimate intergrowth of eldragonite, phase “A” and various other selenides (h.f. $\sim 200 \mu\text{m}$); (f) petrovicite associated with a plethora of other selenium-bearing minerals filling a fracture in krut'aite–penroseite (h.f. $\sim 500 \mu\text{m}$). Abbreviations of mineral names: kps.s. = krut'aite–penroseite solid solution, gru = grundmannite, wat = watkinsonite, cl = clausthalite, pen = penroseite, kl = klockmannite, cha = chalcopyrite, eld = eldragonite, pet = petrovicite, “A” = phase “A” of Paar *et al.* (2012).

and klockmannite) shrinkage cracks or fill interstices in brecciated krut'aite–penroseite solid solutions, the other half formed as independent grains in the matrix. Grundmannite was never observed as inclusions in krut'aite–penroseite.

Grundmannite is non-fluorescent, black and opaque with a metallic lustre and black streak. It is brittle, with an irregular fracture and no obvious parting. Some grains show a perfect $\{001\}$ cleavage. The mean Vickers hardness number (VHN) for a 20 g load is 53 kg mm^{-2} (range 45–61), corresponding to a Mohs hardness of 2 to $2\frac{1}{2}$.

Density could not be measured because of the small grain size, but was calculated at 6.582 g cm^{-3} on the basis of the mean chemical composition and unit-cell parameters derived from the single-crystal X-ray study.

4. Optical properties

In plane-polarized incident light, grundmannite is weakly bireflectant and weakly pleochroic from cream to light grey. The mineral does not show any internal

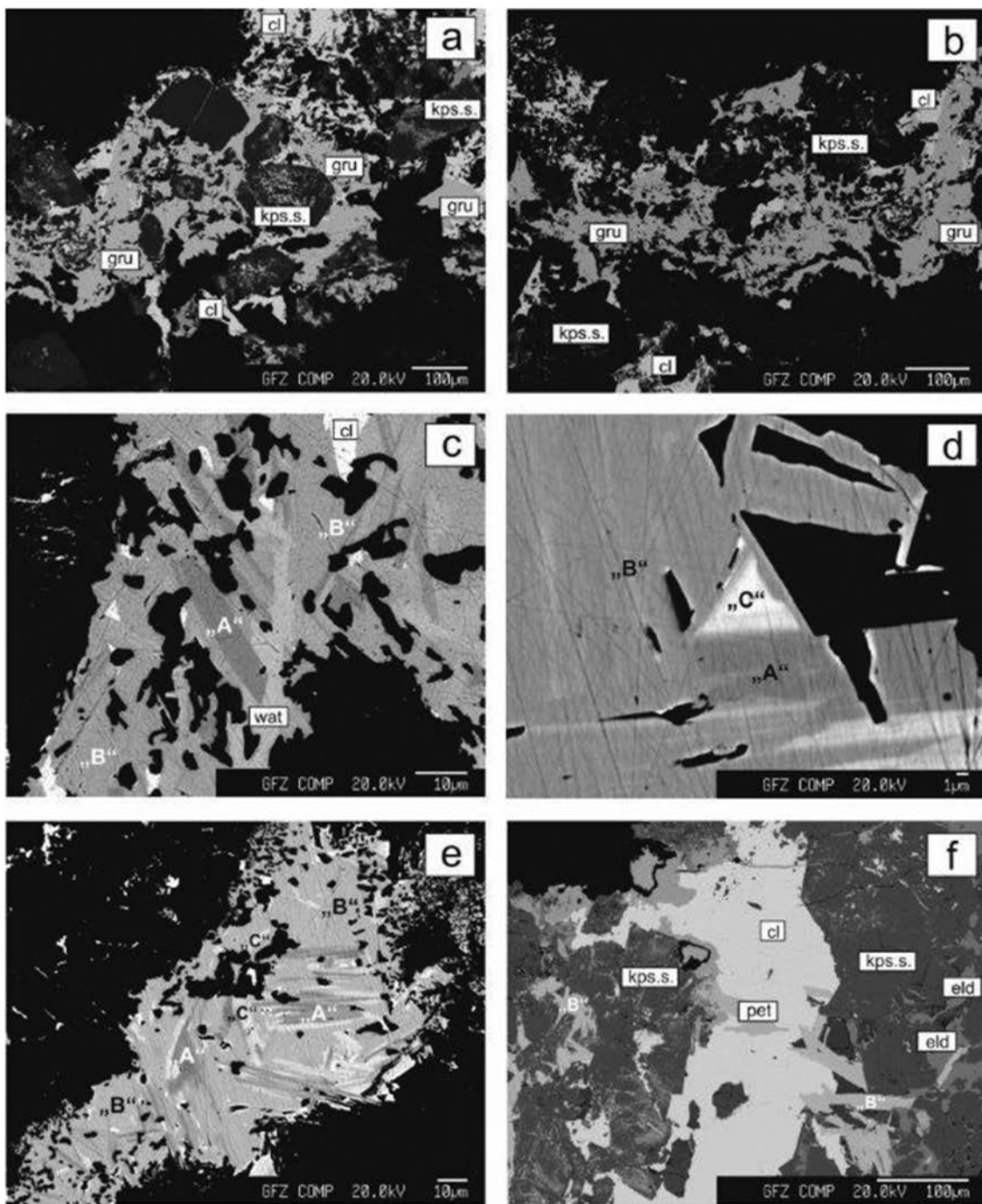


Fig. 2. Microprobe-generated back-scattered electron images of (a) anhedral to subhedral grains of grundmannite (medium bright) and clausthalite (bright) enclosing krut'aité–penroseite crystals; (b) irregularly shaped grundmannite intergrown with clausthalite; (c) intergrowth of phases “A” and “B” with watkinsonite and clausthalite; (d) phases “A”, “B” and “C” (for chemical composition see Table 3) in grain contact; (e) mineral aggregate composed of phases “A” (medium bright), “B” (least bright) and “C” (brightest; for compositional data see Table 4, ana.#4); (f) clausthalite intergrown with petrovicite and inhomogeneous acicular crystals mainly composed of phase “B” filling a fracture in krut'aité–penroseite solid solution, in contrast to eldragónite occurring inside. See Fig. 1 for abbreviations of mineral names.

reflections. Between crossed polarisers, grundmannite is distinctly anisotropic, with light-brown to brown rotation tints.

Quantitative reflectance data for grundmannite were obtained in air relative to a Zeiss WTiC standard using a J & M TIDAS diode array spectrometer attached to a

Zeiss Axiotron microscope. Measurements were made on non-oriented grains at extinction positions leading to designation of R_1 (minimum) and R_2 (maximum). The results are listed in Table 1 (together with the calculated colour values) and illustrated graphically in Fig. 3.

Table 1. Reflectance data and colour values for grundmannite.

λ (nm)	R ₁ (%)	R ₂ (%)	λ (nm)	R ₁ (%)	R ₂ (%)
400	40.7	42.3	640	42.5	46.1
420	40.7	42.6	660	42.5	46.3
440	40.8	42.8	680	42.5	46.5
460	40.9	43.1	700	42.5	46.6
480	41.0	43.6	Commission on Ore Mineralogy wavelengths		
500	41.2	44.1			
520	41.5	44.6			
540	41.8	45.0			
560	41.9	45.3			
580	42.0	45.5	470	41.0	43.4
600	42.2	45.8	546	41.8	45.1
620	42.3	46.0	589	42.1	45.7
			650	42.5	46.2
Colour values					
C illuminant		A illuminant			
	R ₁	R ₂	R ₁	R ₂	
x	0.313	0.316	0.450	0.452	
y	0.319	0.322	0.408	0.409	
Y (%)	41.8	45.1	42.0	45.4	
I _d	577	576	586	586	
P _e (%)	1.7	3.1	2.5	4.4	

5. Chemical composition

Ore minerals from El Dragón were routinely checked for concentrations of Cu, Ag, Pb, Hg, Fe, Co, Ni, As, Sb, Bi, S, and Se. Quantitative chemical analyses of grundmannite and the associated selenides were conducted in wavelength-dispersive (WDS) mode, using a JEOL thermal field-emission-type electron probe X-ray microanalyzer (FE-EPMA) JXA-8500F (HYPERPROBE) at the Deutsches GeoForschungsZentrum GFZ, Potsdam, Germany. The probe was operated at 20 kV, 20 nA; the beam size was 1–2 μm . The counting time on peak was 20 s, with half that time on background on both sites of the peak. Special care was taken to avoid any elemental interferences on peak and backgrounds, or to empirically correct them. The following standards, emission lines and analysing crystals (in parentheses) were used: Cu – synthetic Cu-metal, $K\alpha$ (LIF); Ag – natural naumannite, $L\alpha$ (PETJ); Pb – natural clausthalite, $M\alpha$ (PETH); Hg – natural cinnabar, $L\alpha$ (LIF); Fe – natural pyrite, $K\alpha$ (LIF); Co – natural skutterudite, $K\alpha$ (LIF); Ni – natural pentlandite, $K\alpha$ (LIF); As – natural skutterudite, $L\alpha$ (TAP); Sb – natural stibnite, $L\alpha$ (PETJ); Bi – synthetic Bi₂Se₃, $M\alpha$ (PETH); S – natural sphalerite, $K\alpha$ (PETJ); Se – natural naumannite, $K\alpha$

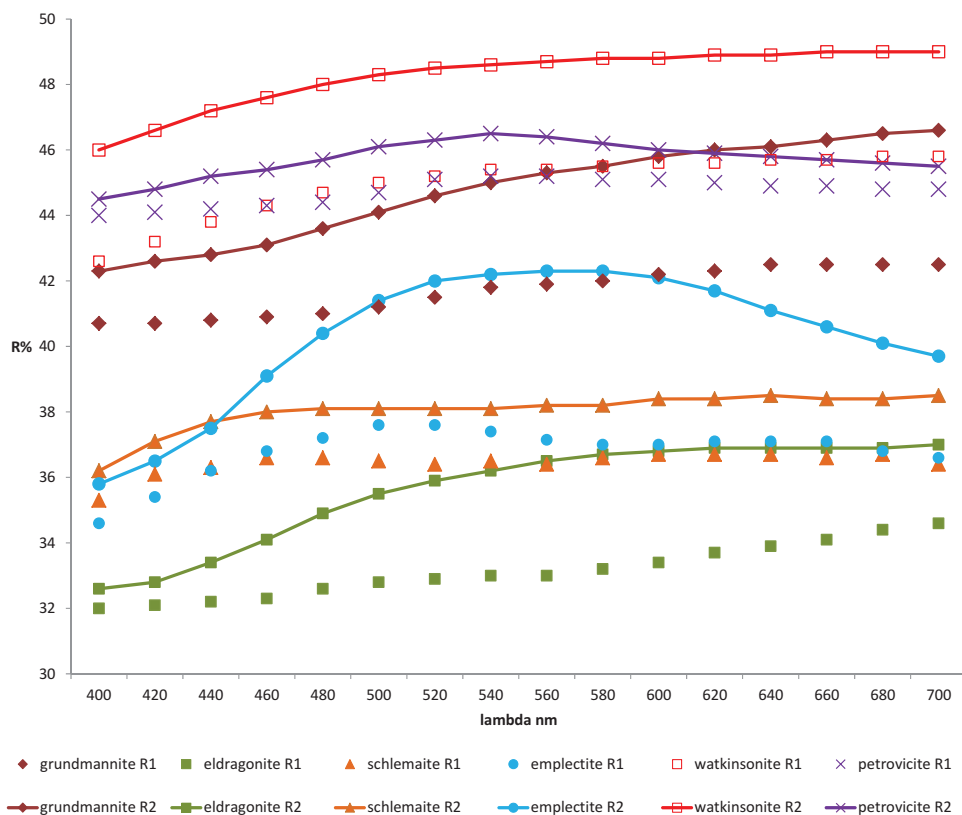


Fig. 3. Reflectance spectra of grundmannite, its S-analogue emplectite, and other Cu–Bi selenides in air. Data sources: eldragónite – Paar *et al.* (2012); schlemaite – Förster *et al.* (2003); emplectite – Criddle & Stanley (1993); watkinsonite – Johan *et al.* (1987); petrovicite – Picot & Johan (1982).

(LIF). The CITZAF routine in the JEOL software, which is based on the $\phi(\rho Z)$ method (Armstrong, 1995), was used for data processing.

5.1. Grundmannite

In this study, grundmannite from El Dragón displays only weak variations in composition (Table 2). In addition to the major cations Cu, Bi and Se, the only other element always present is Pb, with concentrations between 1.0 and 1.3 wt.%. Minor amounts of Hg (< 0.3 wt.%) and Ni (< 0.2 wt.%) were detected occasionally. Substitution of divalent Pb for trivalent Bi explains the observed slight deviation from ideal stoichiometry. The mean empirical formula, normalized to 4 atoms per formula unit (*apfu*), is $\text{Cu}_{0.99}(\text{Bi}_{0.91}\text{Pb}_{0.02})_{\Sigma 0.93}\text{Se}_{2.08}$ ($n = 19$). The ideal formula is CuBiSe_2 , thus being the Se-analogue of emplectite, CuBiS_2 , as confirmed by structural data.

Table 2. Composition of grundmannite (wt.%) from El Dragón.

	Cu	Hg	Pb	Ni	Bi	Se	Total
mean	14.88	0.07	1.23	0.05	44.9	38.92	100.05
1 σ	0.11	0.10	0.10	0.06	0.24	0.24	0.32
min	14.69	0.00	0.99	0.00	44.62	38.44	99.38
max	15.05	0.30	1.38	0.22	45.53	39.33	100.81

Notes: 1 $\sigma = 1\sigma$ standard deviation.

5.2. Associated Cu–Bi–(Pb)–(Hg)–Se minerals

The mean compositions (together with the number of analysed spots) and 1 σ standard deviations and the respective formula proportions for petrovicite, watkinsonite, eldragónite, and unnamed phases “A”, “B” and “C” are listed in Table 3. Except for the newly established phase “C”, the compositional data reported here are slightly different from those measured by Paar *et al.* (2012), but generally confirm the observations and conclusions made by these authors.

Based on 15 *apfu*, petrovicite from the El Dragón mine corresponds to $(\text{Cu}_{2.97}\text{Ag}_{0.04})_{\Sigma 3.01}\text{Hg}_{0.99}\text{Pb}_{0.99}\text{Bi}_{1.03}\text{Se}_{4.98}$, agreeing with its ideal formula $\text{Cu}_3\text{HgPbBiSe}_5$. Silver is omnipresent as a minor element (0.2–0.8 wt.%). As already recognized by Paar *et al.* (2012), the composition of watkinsonite, ideally $\text{Cu}_2\text{PbBi}_4\text{Se}_8$, is characterized by the substitution of variable, but uncommonly large concentrations of Ag for Cu. The concentrations of Ag range between 1.3 and 5.2 wt.%, which is equivalent to 9–44 mol% $\text{Ag}_2\text{PbBi}_4\text{Se}_8$, suggesting the possible existence of an Ag-analogue of watkinsonite in nature. The other omnipresent cation in the watkinsonite microprobe analyses is Hg, with concentrations up to 1.3 wt.%. Nickel occurs sporadically, with maximum concentrations of 0.3 wt.%. Since the crystal-chemical behaviour of Hg, having a linear or a tetrahedral coordination [see, *e.g.*, the mixed (Hg,Ag,Cu) sites in rouxelite (Biagioni *et al.*, 2014a) or in galkhaite (Biagioni *et al.*, 2014b)], could suggest a preferential substitution of Hg at some Cu sites (probably at the Cu1 site), the mean formula of watkinsonite could be

Table 3. Mean composition (wt.%) and formula proportions of Cu–Bi selenides associated with grundmannite.

n	Petrovicite		Watkinsonite		Eldragónite		Phase “A”		Phase “B”		Phase “C”	
	8		39		11		24		28		4	
	Aver.	1 σ	Aver.	1 σ	Aver.	1 σ	Aver.	1 σ	Aver.	1 σ	Aver.	1 σ
Cu	15.51	0.35	5.33	0.83	34.18	0.18	13.34	0.28	9.31	0.43	8.53	0.23
Ag	0.45	0.24	2.62	1.20	0.10	0.05	1.02	0.28	0.73	0.25	2.12	0.20
Hg	16.51	0.19	0.83	0.40	0.01	0.02	7.67	0.22	11.43	0.30	7.08	0.27
Pb	17.12	0.13	12.23	0.43	0.00	0.00	16.87	0.13	13.55	0.24	16.54	0.21
Fe	0.00	0.00	0.01	0.03	1.47	0.23	0.00	0.00	0.00	0.00	0.02	0.03
Co	0.00	0.00	0.00	0.01	0.02	0.04	0.03	0.04	0.03	0.03	0.02	0.02
Ni	0.01	0.03	0.05	0.17	0.21	0.19	0.15	0.15	0.17	0.14	0.12	0.11
Bi	17.80	0.07	44.52	0.68	19.83	0.13	27.65	0.19	31.17	0.26	32.59	0.18
S	0.00	0.00	0.00	0.00	0.00	0.00	0.00	0.00	0.00	0.00	0.00	0.00
Se	32.55	0.11	34.53	0.54	44.33	0.16	33.52	0.20	34.00	0.32	33.75	0.07
Total	99.93	0.50	100.12	0.87	100.16	0.49	100.24	0.30	100.40	0.46	100.76	0.09
<i>apfu</i>	11		15		13		21		12		22	
Cu	2.97	0.03	1.53	0.24	5.71	0.05	4.90	0.09	2.05	0.09	3.45	0.09
Ag	0.04	0.01	0.44	0.21	0.01	0.01	0.22	0.06	0.10	0.03	0.50	0.05
Hg	0.99	0.01	0.07	0.02			0.89	0.03	0.80	0.02	0.91	0.04
Pb	0.99	0.01	1.08	0.03			1.90	0.02	0.91	0.02	2.05	0.02
Fe					0.28	0.04					0.01	0.01
Co						0.01	0.01	0.02	0.01	0.01	0.01	0.01
Ni			0.02	0.02	0.04	0.03	0.06	0.06	0.04	0.03	0.05	0.05
Bi	1.03	0.00	3.88	0.05	1.01	0.01	3.09	0.03	2.08	0.03	4.01	0.03
Se	4.98	0.01	7.98	0.04	5.96	0.03	9.92	0.04	6.01	0.05	11.00	0.03

Notes: $n =$ number of spot analyses averaged, 1 $\sigma = 1\sigma$ standard deviation.

written as (Cu_{1.53}Ag_{0.44}Hg_{0.07}Ni_{0.02})_{Σ2.06}Pb_{1.08}Bi_{3.88}Se_{7.98}, normalized to 15 *apfu*. Taking into account the elevated contents of Ag und Hg, watkinsonite from El Dragón closely resembles watkinsonite from Niederschlema–Alberoda, Erzgebirge, Germany, which has the mean formula (Cu_{1.47}Ag_{0.49}Cd_{0.02}Hg_{0.01}Ni_{0.01})_{Σ2.00}Pb_{1.01}Bi_{3.98}(Se_{7.98}S_{0.05})_{Σ8.03} (Förster *et al.*, 2003).

Our analytical data for phases “A” and “B” confirmed the formula projections made by Paar *et al.* (2012), but yielded analytical totals relatively closer to 100 wt.% (*cf.* Table 3). The mean formula of phase “A”, based on 22 *apfu*, is (Cu_{4.90}Hg_{0.89}Ag_{0.22}Ni_{0.06}Co_{0.01})_{Σ6.08}Pb_{1.90}Bi_{3.09}Se_{9.92}, ideally corresponding to Cu₅Pb₂HgBi₃Se₁₀. Between 0.4 and 1.3 wt.% Ag was substituted for Cu. Nickel is omnipresent, with concentrations between <0.1 and 0.6 wt.%. The Pb deficit (1.90 with respect to ideal 2 *apfu*), coupled with a (Cu,Hg,Ag,Ni,Co) and Bi excess, may be related to a substitution mechanism like Ag⁺+Bi³⁺ = 2Pb²⁺. Normalized to 12 *apfu*, phase “B” has the mean composition (Cu_{2.05}Hg_{0.80}Ag_{0.10}Ni_{0.04}Co_{0.01})_{Σ3.00}Pb_{0.91}Bi_{2.08}Se_{6.01}, corresponding to the ideal formula Cu₂PbHgBi₂Se₆. Like phase “A”, this species contains minor concentrations of Ag (0.4–1.8 wt.%) and Ni (<0.5 wt.%). The analytical data for phase “C” agree with the ideal formula Cu₄Pb₂HgBi₄Se₁₁. The mean empirical formula is (Cu_{3.45}Hg_{0.91}Ag_{0.50}Ni_{0.05}Co_{0.01}Fe_{0.01})_{Σ4.93}Pb_{2.05}Bi_{4.01}Se_{11.00}, based on 22 *apfu*. Noteworthy are the elevated concentrations of Ag (1.8–2.3 wt.%), most probably hosted at the Cu-position(s), and trace amounts of Ni (<0.3 wt.%).

The composition of phase “C” requires additional remarks. This species may be chemically more variable than reflected by its mean composition provided in Table 3 and a single spot analysis presented in Table 4 (ana.#1).

Table 4. Results of spot analyses of phase “C”.

ana.#	1	2	3	4
Cu	8.53	6.51	6.77	6.66
Ag	2.19	3.32	2.29	4.11
Hg	7.32	7.01	7.20	7.22
Pb	16.41	16.39	16.15	16.37
Fe	0.00	0.38	1.43	0.00
Co	0.00	0.09	0.06	0.13
Ni	0.11	0.39	0.25	0.40
Bi	32.43	32.37	33.05	32.55
Se	33.78	33.31	33.30	33.00
Total	100.76	99.77	100.50	100.45
Cu (<i>apfu</i>)	3.45	2.69	2.75	2.74
Ag	0.52	0.81	0.55	1.00
Hg	0.94	0.92	0.93	0.94
Pb	2.04	2.07	2.01	2.07
Fe	0.00	0.18	0.66	0.00
Co	0.00	0.04	0.02	0.06
Ni	0.05	0.17	0.11	0.18
Bi	3.99	4.06	4.08	4.08
Se	11.01	11.06	10.89	10.94

Notes: cations normalized to 4 *apfu*.

Spot analyses performed in relatively brighter domains in intergrowths of phases “A” and “B” also revealed compositions that are characterized by larger concentrations of Fe (up to 1.4 wt.%) or Ni (up to 0.4 wt.%) (Table 4, ana.# 2–4). If these data did not suffer from analytical shortcomings owing to the small domain size and the intimate intergrowth with other selenides, they would also fit the ideal composition Cu₄Pb₂HgBi₄Se₁₁, assuming that Fe, as well as Ni and Co, are hosted at the Cu-position(s), in agreement with the strong negative correlation observed between (Fe, Ni) and Cu. If these compositions refer to phase “C”, one quarter of the Cu-position could be occupied by Ag (Table 4, ana.# 4). Crystal-structure data are required to resolve this problem, for the acquisition of which suitable material was not available.

6. Crystal structure

6.1. X-ray powder-diffraction data

The observed powder diffraction pattern (Table 5) of the same grundmannite fragment used for the single-crystal study (see below) was collected with a CCD-equipped diffractometer Xcalibur PX Ultra using CuK α radiation (50 kV and 40 mA – 5 h exposition time). Crystal-to-detector distance was 7 cm. Data were processed using the *CrysAlis* software package version 1.171.31.2 (Oxford Diffraction, 2006) running on the Xcalibur PX control PC. The unit-cell parameters obtained from powder data, using the software *UnitCell* (Holland & Redfern, 1997), are: $a = 6.6331(2)$, $b = 4.2551(2)$, $c = 15.3782(6)$ Å, $V = 434.04(2)$ Å³, in excellent agreement with those obtained from single-crystal data.

6.2. X-ray single-crystal data

Three grundmannite fragments were mounted on a 0.005 mm diameter carbon fibre (which was, in turn, attached to a glass rod) and checked on a CCD-equipped Oxford Diffraction Xcalibur 3 single-crystal diffractometer, operating with MoK α radiation ($\lambda = 0.71073$ Å). One of them (size: 75 × 80 × 95 μm) showed an excellent diffraction quality and the full data collection was done (Table 6). Intensity integration and standard Lorentz-polarization corrections were performed with the *CrysAlis* RED (Oxford Diffraction, 2006) software package. The program ABSPACK of the *CrysAlis* RED package (Oxford Diffraction, 2006) was used for the absorption correction. Reflection conditions were consistent with the space group *Pnma*, the space group observed for emplectite (Kyono & Kimata, 2005) which can be considered the S-analogue of grundmannite. The full-matrix least-squares program SHELXL-97 (Sheldrick, 2008), working on F^2 , was used for the refinement of the structure, which was carried out starting from the atomic coordinates reported for emplectite (Kyono & Kimata, 2005). Site-scattering values were refined using scattering curves for neutral species (Ibers &

Table 5. Calculated and observed X-ray powder diffraction data for grundmannite.

<i>hkl</i>	d_{calc} (Å)	I_{calc}	d_{obs} (Å)	I_{obs}
002	7.6845	17.11	–	–
102	5.0225	23.10	5.01	15
004	3.8423	18.82	3.83	15
111	3.4901	49.45	3.49	50
104	3.3251	30.54	3.32	70
200	3.3180	57.24	–	–
013	3.2746	100.00	3.27	100
112	3.2479	13.01	3.24	25
201	3.2433	15.30	–	–
202	3.0462	6.29	3.05	5
113	2.9365	7.56	2.940	10
203	2.7849	7.16	2.785	10
015	2.4923	40.52	2.490	45
212	2.4775	8.55	2.478	10
106	2.3897	12.40	2.390	15
213	2.3307	44.97	2.329	50
020	2.1290	33.31	2.128	35
215	1.9927	30.98	1.995	35
017	1.9514	11.64	1.952	10
311	1.9471	31.69	1.946	30
008	1.9211	10.28	1.922	10
304	1.9170	21.83	1.918	20
312	1.9019	5.71	–	–
117	1.8722	11.66	1.874	10
024	1.8622	5.18	–	–
216	1.8306	9.98	1.832	10
124	1.7930	10.56	1.796	10
220	1.7919	20.07	1.790	20
221	1.7798	5.66	–	–
314	1.7480	5.29	–	–
208	1.6626	9.74	1.664	10
126	1.5896	7.13	1.590	5
119	1.5416	11.17	1.542	10
317	1.4634	6.66	1.465	5
028	1.4263	7.51	1.425	25
324	1.4246	15.96	–	–
033	1.3678	7.20	1.368	5
228	1.3103	8.15	1.310	10
233	1.2646	5.82	1.262	15
511	1.2628	9.87	–	–
504	1.2545	7.16	1.253	5
235	1.2012	5.06	–	–
331	1.1910	5.45	–	–
524	1.0808	7.67	–	–

Notes: calculated diffraction pattern obtained with the atom coordinates reported in Table 7 (only reflections with $I_{\text{rel}} \geq 5$ are listed). Intensities calculated using XPOW software version 2.0 (Downs *et al.*, 1993).

Hamilton, 1974) as follows: Cu vs. □ and Bi vs. □ for the cation sites, and Se vs. □ for the anion sites. All sites were found fully occupied, and the occupancy factors were then

Table 6. Data and experimental details for the selected grundmannite crystal.

Crystal data	
Formula	CuBiSe ₂
Crystal size (mm)	0.075 × 0.080 × 0.095
Form	block
Colour	black
Crystal system	orthorhombic
Space group	<i>Pnma</i>
<i>a</i> (Å)	6.6362(5)
<i>b</i> (Å)	4.2581(3)
<i>c</i> (Å)	15.3691(9)
<i>V</i> (Å ³)	434.29(5)
<i>Z</i>	4
Data collection	
Instrument	Oxford Diffraction Xcalibur 3
Radiation type	MoK α ($\lambda = 0.71073$ Å)
Temperature (K)	293(2)
Detector to sample distance (cm)	5
Number of frames	677
Measuring time (s)	60
Maximum covered 2θ (°)	70.00
Absorption correction	multi-scan (ABSPACK; Oxford Diffraction, 2006)
Collected reflections	7621
Unique reflections	818
Reflections with $F_o > 4\sigma(F_o)$	611
R_{int}	0.0257
R_{σ}	0.0546
Range of <i>h, k, l</i>	$-10 \leq h \leq 10, -6 \leq k \leq 6,$ $-24 \leq l \leq 24$
Refinement	
Refinement	Full-matrix least squares on F^2
Final R_1 [$F_o > 4\sigma(F_o)$]	0.0247
Final R_1 (all data)	0.0250
Number of least squares parameters	25
Goodness of Fit	1.175
$\Delta\rho_{\text{max}}$ ($e \text{ \AA}^{-3}$)	1.20 (0.78 Å from Bi)
$\Delta\rho_{\text{min}}$ ($e \text{ \AA}^{-3}$)	−1.33 (1.37 Å from Bi)

fixed to 1.00. The electron density refined at the metal sites is in excellent agreement with the electron-microprobe data (Table 2). Successive cycles were run introducing anisotropic temperature factors for all the atoms leading to $R_1 = 0.0247$ for 611 observed reflections [$F_o > 4\sigma(F_o)$] and $R_1 = 0.0250$ for all 818 independent reflections. Fractional atomic coordinates and isotropic atomic displacement parameters are reported in Table 7 whereas the bond distances are given in Table 8. Structure factors and CIF are freely available online as Supplementary Material linked to this article on the GSW website of the journal, <http://eurjmin.geoscienceworld.org/>.

Table 7. Atom fractional coordinates and displacement parameters (\AA^2) for grundmannite.

atom	<i>x</i>	<i>y</i>	<i>z</i>	U_{11}	U_{22}	U_{33}	U_{23}	U_{13}	U_{12}	U_{eq}
Cu	0.22875(10)	¼	0.82957(5)	0.0216(3)	0.0216(3)	0.0188(3)	0	−0.0003(2)	0	0.0207(1)
Bi	0.23364(3)	¼	0.069531(15)	0.0255(1)	0.0255(1)	0.0230(1)	0	0.0001(1)	0	0.02469(8)
Se1	0.64523(9)	¼	0.10055(4)	0.0319(3)	0.0322(2)	0.0294(3)	0	−0.0001(2)	0	0.0312(1)
Se2	0.85020(10)	¼	0.82089(5)	0.0335(3)	0.0345(3)	0.0314(3)	0	−0.0001(2)	0	0.0331(1)

Table 8. Selected bond distances (Å) and angles (°) for grundmannite.

Cu—Se ²ⁱ	2.4488(10)	Se ¹ⁱⁱⁱ —Cu ⁱⁱⁱ	2.5270(5)
Cu—Se ²ⁱⁱ	2.5157(10)	Se ^{1iv} —Cu ^{iv}	2.5270(5)
Cu—Se ¹ⁱⁱⁱ	2.5270(5)	Se ^{2v} —Cu ^v	2.4488(10)
Cu—Se ^{1iv}	2.5270(5)	Se ^{2vi} —Cu ^{vi}	2.5157(10)
Bi—Se ²ⁱⁱⁱ	2.7711(6)	Se ²ⁱⁱⁱ —Bi ⁱⁱⁱ	2.7711(6)
Bi—Se ^{2iv}	2.7711(6)	Se ^{2iv} —Bi ^{iv}	2.7711(6)
Bi—Se ¹	2.7727(7)		
Se ²ⁱ —Cu—Se ²ⁱⁱ	106.18(3)	Cu ⁱⁱⁱ —Se ¹ —Cu ^{iv}	114.81(4)
Se ²ⁱ —Cu—Se ¹ⁱⁱⁱ	107.00(3)	Cu ⁱⁱⁱ —Se ¹ —Bi	113.52(2)
Se ²ⁱⁱ —Cu—Se ¹ⁱⁱⁱ	110.67(3)	Cu ^{iv} —Se ¹ —Bi	113.52(2)
Se ²ⁱ —Cu—Se ^{1iv}	107.00(3)	Cu ^v —Se ² —Cu ^{vi}	112.26(4)
Se ²ⁱⁱ —Cu—Se ^{1iv}	110.67(3)	Cu ^v —Se ² —Bi ⁱⁱⁱ	120.52(2)
Se ¹ⁱⁱⁱ —Cu—Se ^{1iv}	114.81(4)	Cu ^{vi} —Se ² —Bi ⁱⁱⁱ	99.69(2)
Se ²ⁱⁱⁱ —Bi—Se ^{2iv}	100.40(3)	Cu ^v —Se ² —Bi ^{iv}	120.52(2)
Se ²ⁱⁱⁱ —Bi—Se ¹	95.353(17)	Cu ^{vi} —Se ² —Bi ^{iv}	99.69(2)
Se ^{2iv} —Bi—Se ¹	95.353(17)	Bi ⁱⁱⁱ —Se ² —Bi ^{iv}	100.40(3)

Symmetry codes: (i) $x - 1/2, y, -z + 3/2$; (ii) $x - 1, y, z$; (iii) $-x + 1, -y + 1, -z + 1$; (iv) $-x + 1, -y, -z + 1$; (v) $x + 1/2, y, -z + 3/2$; (vi) $x + 1, y, z$.

7. Results and discussion

7.1. Crystal-chemical remarks

The crystal structure of grundmannite (Fig. 4) is topologically identical to that of emplectite, CuBiS₂ (Kyono & Kimata, 2005), with the two independent S positions

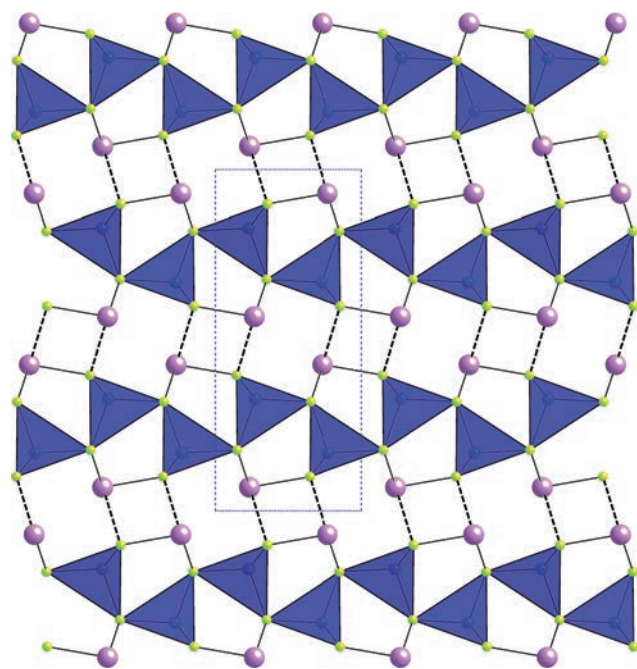


Fig. 4. The crystal structure of grundmannite projected down [010]. The horizontal direction is the a axis. The Cu atoms are depicted as blue tetrahedra, Bi and Se are given as violet and green spheres, respectively. Dashed lines indicate long Bi—Se distances. The unit cell is outlined.

occupied by Se. In the structure, Bi forms BiSe₃ trigonal pyramids (with two additional longer distances) and Cu nearly regular CuSe₄ tetrahedra (Table 8). The entry of Se in the emplectite structure induces a strong enlargement of the unit cell (about 20 % larger than the emplectite unit-cell volume) as well as in the coordination environment of Bi and Cu. Bond valence sums (BVS) have been calculated with the bond parameters given by Brese & O'Keeffe (1991). The BVS values for the metals (1.08 and 2.88 $v.u.$ for Cu and Bi, respectively) are quite satisfactory, whereas the BVS values for the anions deserve some discussion. Se₂ is found to be oversaturated (*i.e.*, 2.32 $v.u.$), in keeping with what is observed also for the emplectite (2.21 $v.u.$) and chalcostibite (2.24 $v.u.$) structures (Kyono & Kimata, 2005). On the contrary, Se₁ is found to be undersaturated (1.64 $v.u.$), a feature that does occur neither for the emplectite (2.06 $v.u.$) nor chalcostibite (2.11 $v.u.$) structures (Kyono & Kimata, 2005). Such an undersaturation could be related to the uncertainties in the determination of the Se position due to some local structural disorder, and be also the cause of the slight undersaturation observed at the Bi site.

The orthorhombic modification of CuBiSe₂ has not yet been synthesized but calculations, using the first-principles DFT method, have shown that such a compound is thermodynamically stable (Kumar & Persson, 2014) and that the chalcostibite – emplectite ($Pnma$) structure is retained. The calculated unit-cell parameters for the CuBiSe₂ compound are $a = 6.58, b = 4.11, c = 15.05$ Å, in close agreement with those measured in this work for grundmannite. The standard thermodynamic properties of CuBiSe₂ were calculated by Babanly *et al.* (2010). The Cu(Sb,Bi)(S,Se)₂ compounds are semiconductors showing orthorhombic symmetry (Kumar & Persson, 2014).

Emplectite and grundmannite are isostructural. Although this could be easily guessed given the similarity of S and Se, there are many phases in the Cu–Ag–S–Se group of minerals that are not isostructural. Amongst this group, acanthite (Ag₂S, space group $P2_1/n$, Frueh, 1958) and naumannite (Ag₂Se, $P2_12_12_1$, Wiegers, 1971) and stromeyerite (CuAgS, $Cmc2_1$, Baker *et al.*, 1991) and eucairite (CuAgSe, $Pmnm$, Frueh *et al.*, 1957) are not isostructural, whereas metacinnabar (HgS, $F-43m$, Aurivillius, 1964) and tiemannite (HgSe, $F-43m$, Earley, 1950) and thalculusite (Cu₂FeTi₂S₄, $I4/mmm$, Makovicky *et al.*, 1980) and bukovite (Cu₂FeTi₂Se₄, $I4/mmm$, Makovicky *et al.*, 1980) are isostructural. As to the IMA sulfosalt systematics (Moëlo *et al.*, 2008), grundmannite is a binary sulfosalt and the third member of the emplectite isotopic series, after emplectite and chalcostibite (CuSbS₂).

7.2. Origin of grundmannite

A reinvestigation of a large collection of ore and country-rock samples from El Dragón provided strong evidence that the available genetic concepts on the origin of this unique mineralization (Grundmann *et al.*, 1990; Paar *et al.*,

2012) require a substantial revision (to be presented elsewhere). The most likely source of Se and accompanying elements (Cu, Co, Ni, Pb, Bi, Ag, ...) is of the *Kupferschiefer*-type: reduced black shale rich in framboidal pyrite, copper sulphides, and organic material. The Se mineralization was deposited in a fault zone at the contact of that shale with a hematite-rich, oxidized siltstone. Our genetic model involves the transport and deposition of Se and accompanying elements from the same low-temperature hydrothermal fluid (likely a heated descending meteoric water) during one single event. Krut'aite–penroseite solid solutions were among the first selenides that crystallized from that solution, thus enriching it in elements incompatible with its structure, mainly Pb, Bi, and Hg. Grundmannite postdates the krut'aite–penroseite solid solutions and appears to also crystallize later than the bulk of accompanying Cu–Bi–(Pb)–(Hg)–Se minerals. Together with later generations of watkinsonite and clausthalite, it constitutes the youngest primary Se-mineral forming the El Dragón deposit, precipitated probably in the stability fields of umangite and klockmannite. Thermodynamic properties and calculated phase equilibria of selenides (Simon & Essene, 1996) permit the fugacities of Se₂ and S₂ during grundmannite crystallization to be broadly constrained. Thus, the absence of berzelianite and bellidoite suggests that the Se fugacity was in a range from below the krut'aite–klockmannite univariant reaction to above the umangite–berzelianite univariant reaction. For a temperature of 100 °C typical for most telethermal vein-type deposits, this range corresponds to log f Se₂ between –10.5 and –14.5 (Simon & Essene, 1997). The presence of hematite/goethite and the absence of chalcopyrite, pyrite and bornite imply maximum S fugacities of roughly log f S₂ ≈ –17, but the actual fugacities most likely were much lower considering the remarkable S paucity of all Se minerals. Thus, the crystallization environment of grundmannite includes a f Se₂/ f S₂ ratio greater than unity and the presence of hematite, conditions typically prevailing during the formation of telethermal vein-type selenide mineralization (Simon & Essene, 1997).

Acknowledgements: First of all, our sincere thanks go to Günter Grundmann, who provided the samples from El Dragón studied in the paper, called the first author's attention to the presence of unidentified minerals in these specimens, and actively supported our work with a pre-inspection of the polished sections by optical microscopy. He, together with G. Lehrberger, F. Grüner and A. Zwicker (Technische Universität München), collected the samples, from which the holotype material was obtained. The study of the El Dragón and Pacajake selenide occurrences was part of the 'International Scientific Cooperation' European Community – Andean Pact Countries, 4 Earth Sciences, Joint Research Project No. 9 'Rare metals in Bolivian ores', managed by G. Morteani (Report: EUR 14495 EN, 1993, ISBN 92-826-4547-9). Dieter Rhede (formerly Deutsches GeoForschungsZentrum GFZ,

Potsdam, Germany) is acknowledged for his valuable support with the electron-microprobe analyses and the effort he spent on improving the analytical routines for the quantitative analysis of complex Se minerals. CJS acknowledges Natural Environment Research Council grant NE/M010848/1 Tellurium and Selenium Cycling and Supply. The comments of František Laufek and one anonymous reviewer helped us in improving the paper.

References

- Armstrong, J.T. (1995): CITZAF: a package of correction programs for the quantitative electron microbeam X-ray-analysis of thick polished materials, thin films, and particles. *Microbeam Anal.*, **4**, 177–200.
- Aurivillius, K. (1964): An x-ray and neutron diffraction study of metacinnabarite. *Acta Chem. Scand.*, **18**, 1552–1553.
- Babanly, N.B., Yusibov, Yu. A., Aliev, Z.S., Babanly, M.B. (2010): Phase equilibria in the Cu–Bi–Se system and thermodynamic properties of copper selenobismuthates. *Russ. J. Inorg. Chem.*, **55**, 1471–1481.
- Baker, C.L., Lincoln, F.J., Johnson, A.W.S. (1991): A low-temperature structural phase transformation in CuAgS. *Acta Crystallogr.*, **B 47**, 891–899.
- Biagioni, C., Bindi, L., Zaccarini, F. (2014a): Crystal chemistry of mercury sulfosalts – galkhaite, (Hg_{5+x}Cu_{1-x})Cs_{1-x}As₄S₁₂ ($x \approx 0$): Crystal structure and revision of the chemical formula. *Can. Mineral.*, **52**, 873–882.
- Biagioni, C., Moëlo, Y., Orlandi, P. (2014b): Lead–antimony sulfosalts from Tuscany (Italy). XV. (Tl–Ag)-bearing rouxelite from Monte Arsiccio mine: occurrence and crystal chemistry. *Mineral. Mag.*, **78**, 651–661.
- Breese, N.E. & O'Keeffe, M. (1991): Bond-valence parameters for solids. *Acta Crystallogr.*, **B47**, 192–197.
- Criddle, A.J. & Stanley, C.J. (1993): Quantitative data file for ore minerals, 3rd Edition. Chapman and Hall/Natural History Museum, London.
- Cunningham, C.A., Aparicio, H.N., Murillo, F.S., Jiménez, N. Ch., Lizca, J.-L.B., McKee, E.H., Erickson, G.E., Tavera, F.V. (1993): The relationship between the Porco, Bolivia, Ag–Zn–Pb–Sn deposit, and the Porco caldera. *US Geol. Surv., Open-File Report 94-238*.
- Downs, R.T., Bartelmehs, K.L., Gibbs, G.V., Boisen, M.B., Jr. (1993): Interactive software for calculating and displaying X-ray or neutron powder diffractometer patterns of crystalline materials. *Am. Mineral.*, **78**, 1104–1107.
- Earley, J.W. (1950): Description and synthesis of the selenide minerals. *Am. Mineral.*, **35**, 337–364.
- Förster, H.-J., Cooper, M.A., Roberts, A.C., Stanley, C.J., Criddle, A.J., Hawthorne, F.C., Laflamme, J.H.G., Tischendorf, G. (2003): Schlemaitte, (Cu,□)₆(Pb,Bi)Se₄, a new mineral species from Niederschlema–Alberoda, Erzgebirge, Germany: description and crystal structure. *Can. Mineral.*, **41**, 1433–1444.
- Förster, H.-J., Tischendorf, G., Rhede, D. (2005): Mineralogy of the Niederschlema–Alberoda U–Se–polymetallic deposit, Erzgebirge, Germany. V. Watkinsonite, nevskite, bohdanowiczite, and other bismuth minerals. *Can. Mineral.*, **43**, 899–908.
- Frueh, A.J., Jr. (1958): The crystallography of silver sulfide, Ag₂S. *Z. Krist.*, **110**, 136–144.

- Frueh, A.J., Jr, Czamanske, G.K., Knight, Ch. (1957): The crystallography of eucairite, CuAgSe. *Z. Krist.*, **108**, 389–396.
- Grundmann, G., Lehrberger, G., Schnorrer-Köhler, G. (1990): The El Dragón mine, Potosí, Bolivia. *Mineral. Rec.*, **21**, 133–146.
- Holland, T.J.B. & Redfern, S.A.T. (1997): UNITCELL: a nonlinear least-squares program for cell-parameter refinement and implementing regression and deletion diagnostics. *J. Appl. Crystallogr.*, **30**, 84–84.
- Ibers, J.A. & Hamilton, W.C. Eds. (1974): *International Tables for X-ray Crystallography*, vol. IV. Kynock, Dordrecht, The Netherlands, 366 p.
- Johan, Z., Picot, P., Ruhlmann, F. (1987): The ore mineralogy of the Otish Mountains uranium deposit, Quebec: skippenite, Bi₂Se₂Te, and watkinsonite, Cu₂PbBi₄(Se,S)₈, two new mineral species. *Can. Mineral.*, **25**, 625–638.
- Kumar, M. & Persson, C. (2014): Cu(Sb,Bi)(S,Se)₂ as indium-free absorber material with high optical efficiency. *Energy Procedia*, **44**, 176–183.
- Kyono, K. & Kimata, M. (2005): Crystal structures of chalcostibite (CuSbS₂) and emplectite (CuBiS₂): Structural relationship of stereochemical activity between chalcostibite and emplectite. *Am. Mineral.*, **90**, 162–165.
- Makovicky, E., Johan, Z., Karup-Møller, S. (1980): New data on bukovite, thalcusite, chalcohallite and rohaite. *N. Jb. Miner. Abh.*, **138**, 122–146.
- Mills, S. J., Kampf, A.R., Christy, A.G., Housley, R. M., Thorne, B., Chen, Yu-Sheng, Steele, I. M. (2014): Favreauite, a new selenite mineral from the El Dragón mine, Bolivia. *Eur. J. Mineral.*, **26**, 771–781.
- Moëlo, Y., Makovicky, E., Mozgova, N.N., Jambor, J.L., Cook, N., Pring, A., Paar, W., Nickel, E.H., Graeser, S., Karup-Møller, S., Balic-Žunic, T., Mumme, W.G., Vurro, F., Topa, D., Bindi, L., Bente, K., Shimuzu, M. (2008): Sulfosalt systematics: report of the sulfosalt-subcommittee of the IMA Commission on New Minerals. *Eur. J. Mineral.*, **20**, 7–46.
- Niedermayr, G., Bernhard, F., Bojar, H.-P., Brandstätter, F., Ettinger, K., Moser, B., Paar, W.H., Postl, W., Taucher, J., Walter, F. (1997): Neue Mineralfunde aus Österreich XLVI. *Carintia II*, **187**, 169–214.
- Oxford Diffraction (2006): *CrysAlis RED* (Version 1.171.31.2) and *ABSPACK* in *CrysAlis RED*. Oxford Diffraction Ltd, Abingdon, Oxfordshire, England.
- Paar, W.H., Cooper, M.A., Moëlo, Y., Stanley, C.J., Putz, H., Topa, D., Roberts, A.C., Stirling, J., Raith, J.G., Rowe, R. (2012): Eldragónite, Cu₆BiSe₄(Se)₂, a new mineral species from the El Dragón mine, Potosí, Bolivia, and its crystal structure. *Can. Mineral.*, **50**, 281–294.
- Picot, P. & Johan, Z. (1982): Atlas of Ore Minerals. Elsevier/BRGM.
- Sheldrick, G.M. (2008): A short history of SHELX. *Acta Crystallogr.*, **A64**, 112–122.
- Simon, G. & Essene, E.J. (1996): Phase relations among selenides, sulphides, tellurides, and oxides: I. Thermodynamic properties and calculated equilibria. *Econ. Geol.*, **91**, 1183–1208.
- Simon, G. & Essene, E.J. (1997): Phase relations among selenides, sulphides, tellurides, and oxides: II: Applications to selenide-bearing ore deposits. *Econ. Geol.*, **92**, 468–484.
- Wieggers, G.A. (1971): The crystal structure of the low-temperature form of silver selenide. *Am. Mineral.*, **56**, 1882–1888.
- Zhuze, V.P., Sergeeva, V.M., Shtrum, E.L. (1958): New semiconductor compounds. *Zh. Tekhnich. Fiziki*, **28**, 233–236.

Received 19 August 2015

Modified version received 14 September 2015

Accepted 23 September 2015